

Advanced Lifetime Tests of Plastic Gears with E- and S-Geometry



Gorazd Hlebanja, Matija Hriberšek, Miha Erjavec, and Simon Kulovec

Abstract Plastic gears became inevitable in many industries, numerous material pairs are available to fit any design needs. Material data bases and data sheets information is insufficient in this context, so on-site testing is necessary. Many applications use steel pinions and plastic gear, e.g., in speed reducers, where the pinion can be rather small, and they can run dry. Therefore, a combination alloy steel/POM became of interest and S-N diagrams were determined experimentally on testing rigs in company's lab, which are presented briefly. Yet another consideration is improved gear geometry; S-gears are proposed in this paper due to their experimentally proven qualities. Some information on this gear type is provided. Lifetime tests for this material combination and both gear types are shown in a diagram. It was also shown that the process temperatures never exceed permanent temperature limit of POM. Optical observations show several developed failure mechanisms. However, to assess quantitative wear levels a 3D measuring microscope is used.

Keywords S-gears · E-gears · Wear characterization · Fatigue · Lifetime tests

1 Introduction

Plastic gears are becoming crucial not only in consumer industries but also in quality demanding industries, e.g., in precision or medical devices, and even in power applications. It is almost unnecessary naming their qualities (like low mass and inertia,

G. Hlebanja (✉)

University of Novo Mesto, Na Loko 2, Novo Mesto, Slovenia

e-mail: gorazd.hlebanja@siol.net

G. Hlebanja · M. Hriberšek · M. Erjavec · S. Kulovec

Podkrižnik d.o.o., Lesarska c. 10, Nazarje, Slovenia

e-mail: matija.hribersek@podkrižnik.si

M. Erjavec

e-mail: miha.erjavec@podkrižnik.si

S. Kulovec

e-mail: simon.kulovec@podkrižnik.si

vibration dampening, running without external lubrication, etc.). However, their problems are thermal stability, precision of moulded parts, lower load, etc. On the other side, new materials with improved characteristics are emerging with increased rate. So, to design such gear pairs optimally, their fatigue data are becoming vital, whereas such data are unknown without experimental support. To summarize, there is a lack of reliable data in this context, even similar materials can differ, and various additives even enlarge this difference. So, a possibility to test gear pairs, made of potential material combination, on site can be the advantage for a company since it makes possible faster and independent evaluation and optimal material combination for each application. It is necessary to assess materials in terms of their mechanical, thermal and tribological properties. Despite many data can be extracted from material data sheets, the fatigue life of a gear pair depends on geometry, loading conditions, materials, working temperature, etc., which all originate from a particular application and its scenario. Such data are essential in plastic gear design.

The paper presents experimental results of lifetime tests under prescribed load conditions for selected combinations of thermoplastic gear pairs. Tests were repeated several times to gain statistically relevant result. Testbenches used in this context enabled controlled rotational speed and torque, whereas the spot temperature was monitored by a thermal camera.

The material combination of interest was alloy steel driving gear and driven POM (H) gear. Tests were produced for both, the involute and S-gear geometry. Results of this material combination shows an obvious advantage of S-gears in terms of durability. Data were imported in the KissSoft gear design software (for involute gears). This enabled the determination of Wöhler curves for these material combinations for root/flank areas. E-gears suffered a high temperature rise for the material combination steel and POM at high loads, which is due to highly deformed plastic gear teeth. A tip relief was proposed for E-gears for the next cycle of testing. Also, a 3D scanning topography was used to evaluate wear of tested gears.

2 Properties of the S-Gears

Many papers discussed various aspects of S-gears: the way they are defined [1], possibilities to design and produce various gear types (e.g., helical, crossed, worm gears, planetary gears, etc.) [2], radii of curvature, contact pressure, relative and sliding velocities, oil thickness, (initial) pressure angles, contact stress, etc. [3–5], thermal properties [6]. How do S-gears differ from the involute gears was also discussed in these papers. Important properties of S-gears can be summarized below:

1. Two parameters defining the rack flank curve can be used to modify gear tooth shape to improve its design, e.g., to acquire proper pressure angle, increase tooth root thickness, etc.
2. Cylindrical spur S-gears can operate with a low number of teeth down to 6 or even 4.

3. S-gears exhibit convex-concave contact in the vicinities of the meshing start and end zones.
4. S-gears feature comparatively higher radii of curvature, which implies lower contact pressure.
5. S-gears develop higher contact oil film thickness, which is due to higher relative velocities in the contact.
6. S-gears exhibit relatively longer dedendum part of a pinion tooth flank (comparing to the involute gear) which is meshing with a gear addendum. Difference between the pinion dedendum length and the gear addendum length indicates amount of sliding. And less sliding implies less frictional work and less developed heat, which is of special importance for plastic gears.

As stated in [1], S-gears are defined through the rack profile $y(x)$, where a coordinate system origin lies in the kinematic pole C:

$$y(x) = \begin{cases} a_p m \left(1 - \left(1 - \frac{x}{m}\right)^n\right), & x \geq 0 \\ -a_p m \left(1 - \left(1 + \frac{x}{m}\right)^n\right), & x < 0 \end{cases} \quad (1)$$

and $\lim_{x \rightarrow 0^+} y'(x) = \lim_{x \rightarrow 0^-} y'(x)$. x, y are Cartesian coordinates of the rack profile, m is module in mm, whereas factors a_p and n , namely the height factor and the exponent act as form factors, which affect the tooth shape properties. And the module acts as a scaling factor. The definition of the rack in Eq. (1) is necessary due to the half symmetry of the profile. The rack tooth can be regarded as a cutting tool.

The trigonometric procedure defining the path of contact and gears of an arbitrary number of teeth was described in detail in [1]. This procedure is valid for external as well as for internal gears. So, for an arbitrary point P on the rack tooth flank a unique point U on the path of contact is defined, provided that the normal to the rack profile curve in U passes through C. Similarly, a single point on a flank of a gear with an arbitrary defined number of teeth is produced. The transformations from the rack profile flank through the path of contact to gear flanks are bijective, that is they always give the same rack flank in the reverse direction. These transformations could also have been represented by object translations and rotations in appropriate coordinate systems, of course by employing the basic law of gearing.

As already stated, the gear flank and tooth shape influencing factors are a_p and n , however, one of them can be replaced by the initial pressure angle α_{w0} . Two gear pairs are shown here to illustrate the tooth shape variability in Fig. 1, both with $z_p = 10$ and $z_w = 30$. The first gear pair is with $\alpha_w = 22^\circ$ and $a_p = 1.3$ and the second one with $\alpha_w = 18^\circ$ and $a_p = 1.5$. All gears were designed with the module $m = 50$ mm and since the module acts only as a scaling factor, its size is of no importance in this context. Both rack profiles do not differ much, apart from the inclination and corresponding pressure angles. But the derived paths of contact apparently differ in their length and curvature in the meshing starting and end zones, as it can be observed in Fig. 1. The active parts of both paths of contact delimited by gear tip circles are designated as $\widetilde{A_1E_1}$ and $\widetilde{A_2E_2}$. So, for the higher pressure angle, the path of contact shortens and becomes more curved and inversely (longer and less curved path of

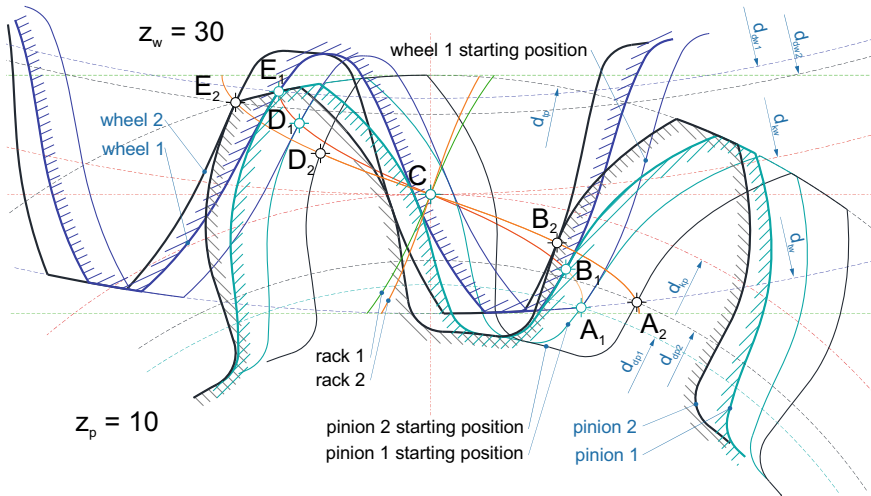


Fig. 1 Gear pair forms with pinion $z_p = 10$ and wheel $z_w = 30$. The generating rack 1 with (initial) pressure angle $\alpha_w = 22^\circ$ and rack 2 with $\alpha_w = 18^\circ$

contact) for lower pressure angles. The tooth root becomes stronger and tooth tip thinner for the larger pressure angle and inversely for smaller pressure angles. The active length of the path of contact \widetilde{AE} , the length \widetilde{AD} which corresponds to the base pitch and the contact ratio are collected in Table 1.

The mating gear teeth flanks start meshing with the pinion dedendum tip and the gear addendum root and proceed from the meshing start to the kinematic pole C and to the pinion addendum and the gear dedendum from C towards the meshing end point. The contact is propagating on the path of contact by rolling and sliding. The active size of the pinion dedendum is smaller than that of the gear addendum. This implies amount of sliding of the addendum on the shorter pinion dedendum, which can be deducted from Fig. 2, which represents the racks, the paths of contact, and the mating flanks of the S- and the E-gear pair. Amount of sliding also implies thermal impact. In general, the dedendum-addendum size difference depends on module, number of teeth, pressure angle. For S-gears the said difference also depends on forming factors—the height and the exponent. The size difference in the case of S-gears is comparatively more convenient, so less sliding is produced along the contact propagation compared to the involute case. The starting pressure angle for the S-gears is 18° and that of the E-gears 20° , and both gears with the same number of teeth, $z = 20$. As Fig. 2 implies:

Table 1 Path of contact characteristics for the S-gear pairs ($z_p = 10, z_w = 30, m = 50$ mm)

Initial pressure angle α_{w0}	18	22
Active length, $l_{\widetilde{AE}}$ [mm]	190.7	162.92
Base pitch, $l_{\widetilde{AD}}$ [mm]	148.2	144.5
Contact ratio, ε []	1.29	1.13

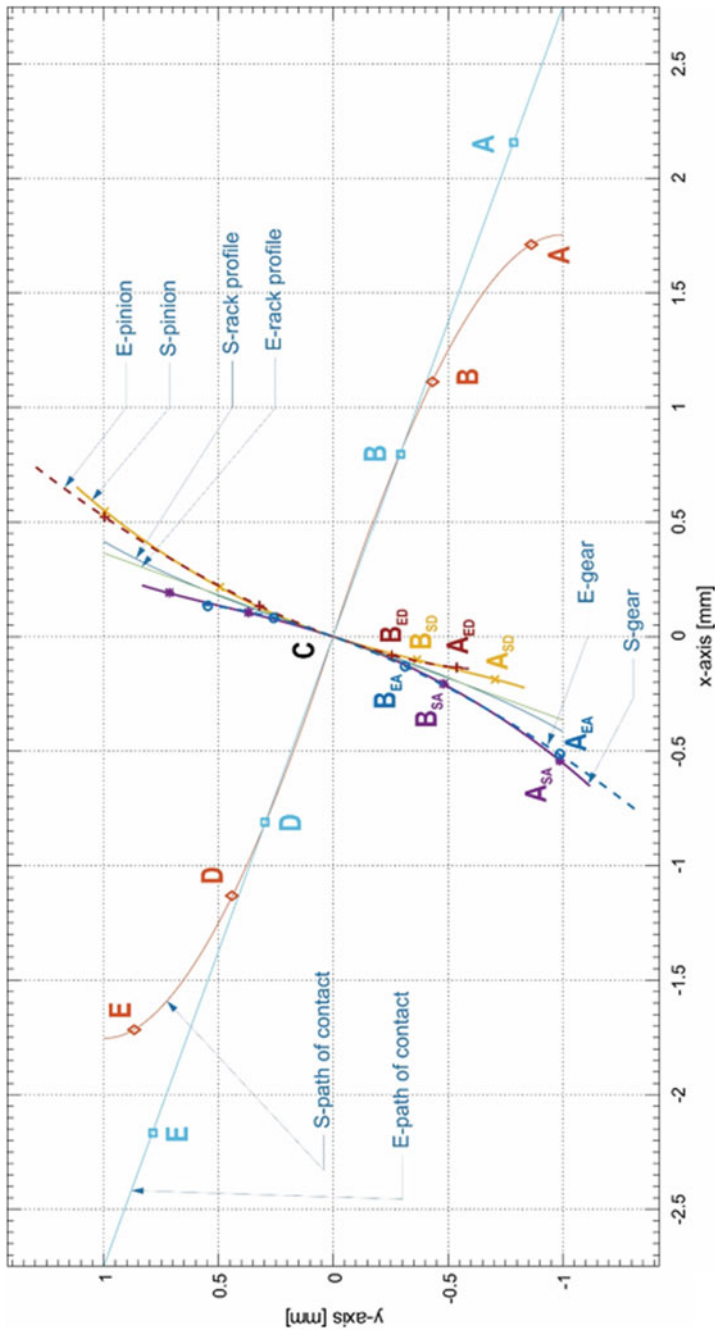


Fig. 2 Comparison of the E and S paths of contact, rack profiles and mating pinion and gear flanks, $m = 1$ mm, $z_p = z_w = 20$, $\alpha_{wE} = 20^\circ$, and $\alpha_{wS} = 18^\circ$

$$\Delta l_E = l(\widetilde{\mathbf{A}_{EA}\mathbf{B}_{EA}}) - l(\widetilde{\mathbf{A}_{ED}\mathbf{B}_{ED}}) > \Delta l_S = l(\widetilde{\mathbf{A}_{SA}\mathbf{B}_{SA}}) - l(\widetilde{\mathbf{A}_{SD}\mathbf{B}_{SD}}) \quad (2)$$

Near the meshing start point, involute gears feature small radii of curvature of the driving pinion and rather high radii of curvature of the driven gear, which implies high sliding velocities in this area. This phenomenon can be observed also in Fig. 2, whereas it becomes distinct when the numbers of teeth are notably apart.

The normal force F_N is transmitted through the contact, which causes the force of friction F_{fr} oriented tangentially to the contact and the corresponding power of friction, $P_{fr} = \mu F_N v_g$. The power of friction generated in the contact representing losses transforms to the heat flow, distributed to both involved flanks. A greater part of the heat is therefore distributed to the slower driving gear and the rest to the longer contacting area of the driven gear. The friction force grows to high levels already at the meshing start, which negatively influences (braking) the contact point velocity along the path of contact and induces negative sliding on the driving gear flank.

Based on the S-gear rack profile, the path of contact, the pinion and inner or outer gear can be calculated by a program. The same program was improved to enable calculation of power, work, flank pressure, contact width, velocities, and flash temperatures. All the parameters can be represented along the path of contact or the active flank profile. Power of friction is therefore given by:

$$P_{fr} = \mu \cdot F_N \cdot v_g = (\mu \cdot F_t / \cos \alpha_w) \cdot v_g \quad (3)$$

The work of friction along the active contact from the meshing start in A in time $t_A = 0$ to the meshing end in E (t_E) is given by:

$$A_{fr} = \sum_{t_A}^{t_E} P_{fri} \cdot \Delta t_i \quad (4)$$

So, the frictional work in a single pinion rotation is $z_p \cdot A_{fr}$, and multiplied by the rotational frequency frictional work accomplished in a minute $\nu \cdot z_p \cdot A_{fr}$. The average frictional power is then $P_{frav} = \nu \cdot z_p \cdot A_{fr}/60$. Table 2 collects data for torque 1.5 Nm for both, E- and S-spur gear pairs with $m = 1$ mm, $z_p = z_w = 20$, $\alpha_{wE} = 20^\circ$, $\alpha_{wS} = 18^\circ$, and $b = 6$ mm and steel/POM material combination. Values for E-gears are higher for 25%.

Table 2 Frictional work and average frictional power for S- and E- gear pair ($z_p = z_w = 20$, $m = 1$ mm, $T = 1.5$ Nm, $\nu = 1400 \text{ min}^{-1}$, $P_t = 219.9$ W)

	S-gears	E-gears
Work in a single contact [J]	0.0135	0.0169
Work in a single rotation [J]	0.2697	0.3389
Work in a minute [J]	377.6	474.5
Average frictional power [W]	6.294	7.909

3 Experimental Arrangement and Tested Gears

Material combinations for gear pairs to be tested are based on existing and potential applications. Due to importance of optimal material selection the company decided to develop and produce own testbenches. The necessity to acquire comparable results which could be input for plastic gear design software, a testbench according to VDI 2736, Part 4 [7] was designed and manufactured. This device is already in trial operation. Nevertheless, smaller devices proved to be useful and were used in this set of experiments. Based on test duration and rotational speed of the selected thermoplastic gears, lifetime cycles were calculated and imported together with flank/root temperature into KISSsoft Software, module Plastics Manager [8]. Based on the processed input data in Plastics Manager, Wohler Curves (S-N) for a selected material combination were obtained. After each experimental lifetime test, the wear characterization has been performed according VDI 2736, Part 2 [9] with Alicona device and evaluation of the gear failure mode. Wear was as well evaluated during testing to acquire wear development data along gear tooth flank.

3.1 Gear Geometry

Small spur S- and E-gears of module 1 mm, width 6 mm, both gears with 20 teeth, were used in these tests. Figure 3 shows their geometrical features. The pinion material in this experimental series was 42CrMo4 QT, alloy steel. Plastic gears were made of acetal homopolymer POM H. Technical data of gears are presented in Table 3. The pressure angle for S-gear in this case amounts to 26.8° in the meshing start point, decreases to 20° in C, and gradually increases to 26.8° for an ideal contact (Fig. 2).

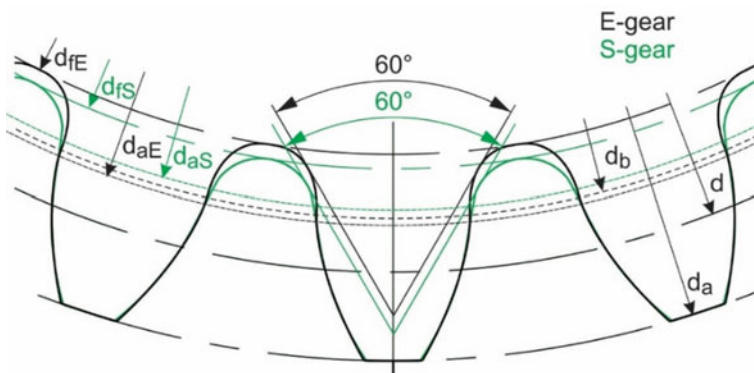


Fig. 3 Comparison of actual E and S gears provided for testing

Table 3 Basic data on S and E gears

Gear type	E-gears	S-gears
Pressure angle α [°]	20	18
Tip diameter, d_a [mm]	22	22
Reference diameter, d [mm]	20	20
Root diameter, d_f [mm]	17.4	17.7
Base diameter, d_b [mm]	18.79	–
Dedendum limit, d_{act} [mm]	18.95	18.59
Critical section s_{fn} [mm]	1,88	1,96

Table 4 Roughness and quality data of metal gears

Gear type	E-gear		S-gear	
	Left	Right	Left	Right
Arithmetic mean deviation R_a [μm]	0,16	0,255	0,187	0,206
Maximum height of the profile, R_z [μm]	1,08	2,27	1,28	1,36
Profile Q (DIN 3961/62)	6	4	5	7
Lead Q (DIN 3961/62)	5	5	7	6
Cumulative pitch F_p (DIN 3961/62)	4	4	1	1

As Fig. 3 and Table 3 disclose, E-gears (for these data) have smaller root, a bit thinner tooth and a bit thicker tip. It is also important that the active dedendum side of S-gears is larger.

Since metal gear surface roughness influences wear, corresponding data, inclusive gear quality according to DIN 3961/62 are presented in Table 4.

Manufacturing means of plastic gears can be injection moulding or cutting. Cut gears are of industrial interest for smaller lots and when a more precise tooth flank shape is prescribed or if alternative gear tooth flanks are of interest. Comparing cut and moulded gears of the same module and number of teeth by measurements of the quality Q according to DIN 3961/62 discloses at least for two grades higher Q of cut gears. Measuring gears on Wenzel GearTec coordinate measurement machine in our case showed the difference of two quality grades in favour of cut gears [10]. So, the quality of cut plastic gears is $Q = 8 \dots 9$ and that of moulded $Q = 10 \dots 11$, which also depends on a cutting tool. Basic disks made of POM without fillers are injection moulded, using an axial sprue enabling higher material flow to gain quality uniform physical characteristics. Disks are then cut by a HSS cutting hob on the CNC Koepfer machine tool as to enable effective manufacturing.

3.2 Experimental Arrangement

Testing results presented in this paper are based on experiments performed on two small testing rigs, which were used to acquire gear durability data. The testing rig is illustrated in Fig. 4. It consists of a framework on which two 4 poles asynchronous squirrel cage electro-motors ($P = 0.37 \text{ kW}$ and $M = 1.8 \text{ Nm}$) are mounted. On the motor rear side two fans are mounted to remove redundant heat. Two small gears are mounted in such a way to precisely adapt centre distance. Power transmission from the motors to the shafts is by belts. Motors are controlled by two frequency inverters which acquire proper rotational frequency and load. The testing rig was calibrated based on laser measurement of shaft deformations with prescribed excitation frequency differences between both inverters. Based on shaft torsional deformation, torque, which is controlled based on current measurement, was calculated. A PLC based counter measures experiment duration time. The testing rig stops when gear failure appears. This is conditioned by nominal current drop for 5%.

It is important to have possibility of measuring contact temperature by a fast thermal camera, so the testing device was designed in such a way to enable frontal view. So, measurements of spot temperatures and temperature field of meshing gears were provided by a thermal camera Optris Xi80. Spot temperature was acquired during entire loading cycle of the lifetime tests, which was facilitated by Optris PIX Connect software.

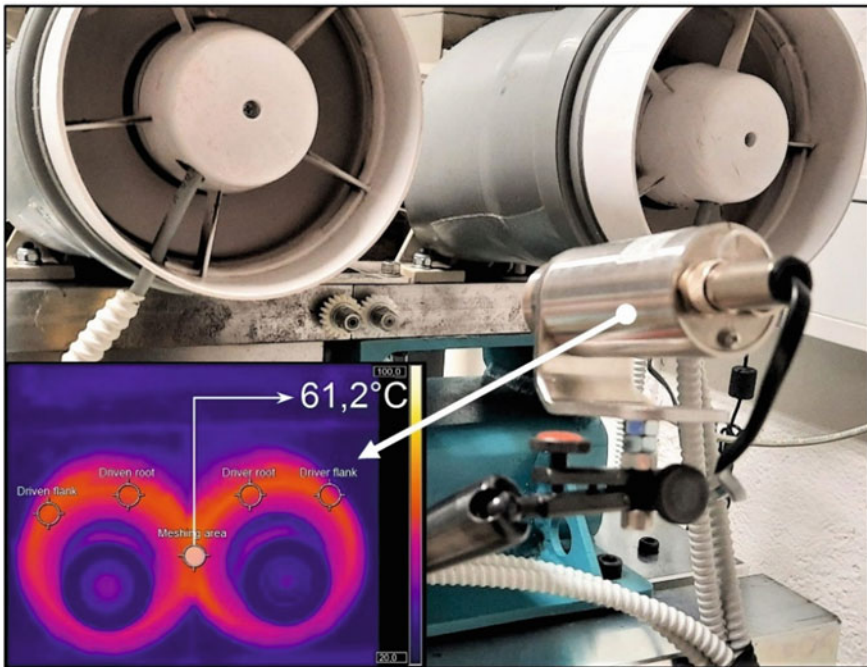


Fig. 4 Testing rig with the thermal camera focusing on a gear pair

4 Experimental Results

Lifetime gear tests were performed under standard environmental conditions with a temperature of 23 °C and a relative humidity of 50%. The experiments were performed at three different load levels, i.e., torques (1.5; 1.3; 1.1 Nm) at the same rotational frequency of the driving and driven gear, which was 1400 rpm. The selection of torques was furthermore based on the preliminary lifetime testing of different types of polymer gears reported in [11]. A computer program for temperature visualization was used to represent the average temperature in the meshing zone during testing. At the end of the test, an evaluation of the average temperature at which a gear failure occurred, was completed.

4.1 Lifetime Tests—Wöhler Diagrams

Many material pairs were submitted lately to lifetime tests, mostly based on acetal and nylon materials, with and without fillers [11, 12]. As already stated, this experimental set is focused on alloy steel (42CrMo4 quenched and tempered) driver, and acetal driven gear.

Wöhler diagrams, plotted based on achieved numbers of cycles in three load levels with three repetitions, are presented in Fig. 5. Results show better performance of

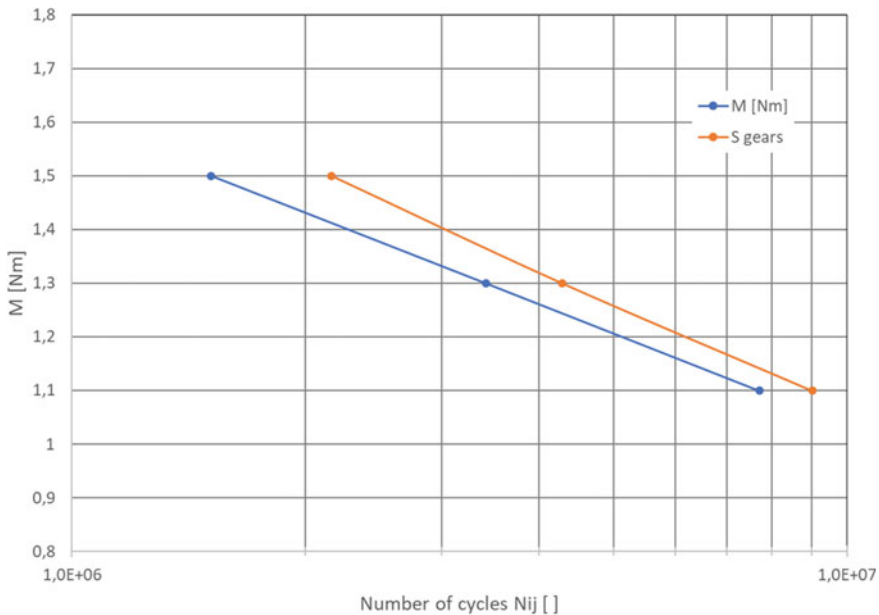


Fig. 5 Comparison of lifetime tests for alloy steel/POM E and S gears

S-gears, which is based on already discussed S-gear properties. This is especially notable with highly loaded gears. Similar results were gained in several attempts, various material combinations and in different labs, e.g., [13, 14]. In the research [13] it was also discovered that S-gears (POM/POM) have better thermal performance with lower loads, below 1 Nm.

An important aim of performing durability tests of thermoplastic gears is exportation of acquired temperature data (tooth flank and root) and lifetime test data, material mechanical and thermal properties, and temperature dependent modulus of elasticity into the program system KISSsoft plastic manager and build the material base, which then aids in building an advanced model to search an optimal solution for a particular application.

4.2 Thermal Measurements

Thermal camera was used to monitor and record spot temperatures of the loaded gear pair in operation. The available Optris Xi80 camera acquires the highest temperature in a 2×2 mm spot. The meshing zone, the driver flank and root, and the driven flank and root spot temperatures were observed in this research. This is diagrammatically presented for the involute gear pair with load 1,5 Nm in Fig. 6.

The courses of temperatures clearly distinguish between the metal driver and driven plastic gear. Temperatures are significantly higher for the plastic gear. The temperature-time (number of cycles) dependency consists of three main sections, which are: (a) running-in area where thermoplastic driven gear fits to steel gear in

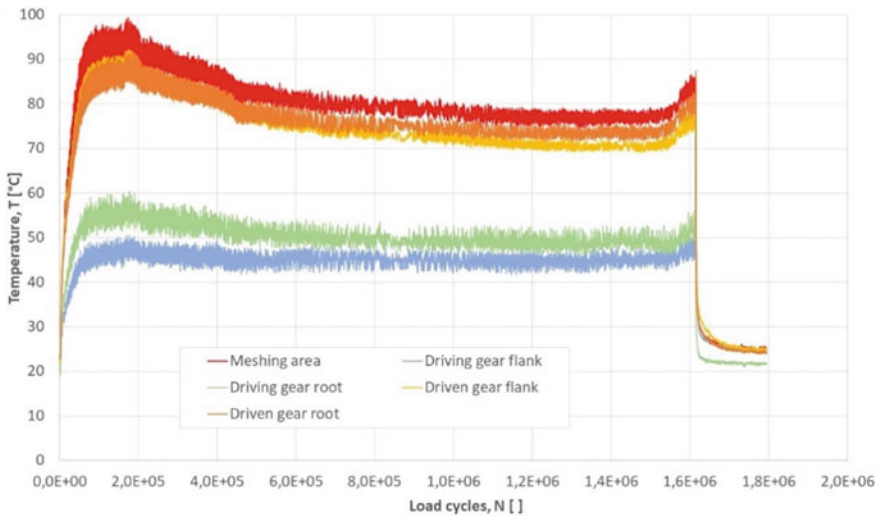


Fig. 6 Temperature-number of cycles (time) profiles for the E-gear pair loaded by 1.5 Nm

terms of tooth flanks; (b) a phase of a quasi-stationary operating at stable temperature; (c) a phase of increasing gear wear that, in combination with fatigue, causes failure of the thermoplastic gear. These phases are clearly distinguished in Fig. 6, which, beside meshing spot, also shows temperature diagrams of flank and root spots for both, the driver, and the driven gear.

Thermal behaviour of steel/POM gear pairs was discussed in [15] and it was observed that E-gear pair at 1.5 Nm exhibits an extraordinary temperature peak during running-in phase. This phenomenon can be attributed to the unmodified involute tooth tip profile and plastic gear tooth deformation due to a high load [16], whereas the steel gear can be regarded as a rigid body in this context. So, a driven gear suffers an additional impact at a meshing start point A and the temperature rise. The consequence is rather high initial wear of a driven plastic gear. The solution of this problem can be tip relief. No such trend during running-in phase was observed at lower load levels for E-gears. S-gears do not exhibit such temperature rise at all.

In the next phase, relatively stationary conditions prevail. For E gears the initially high temperature drops and prevails until the final phase. Uniform wear occurs in this phase for both gear types, thermal camera snapshots are shown in Fig. 7. The last phase of the lifetime test shows significant changes of the gears. This is due to the increased wear above the critical limit in connection with the fatigue of the material, which causes degradation of the bonds between the molecules in the material and the subsequent teeth failure. Process temperatures do not increase up to the constant working limit, which is for POM between 90 and 100 °C [17].

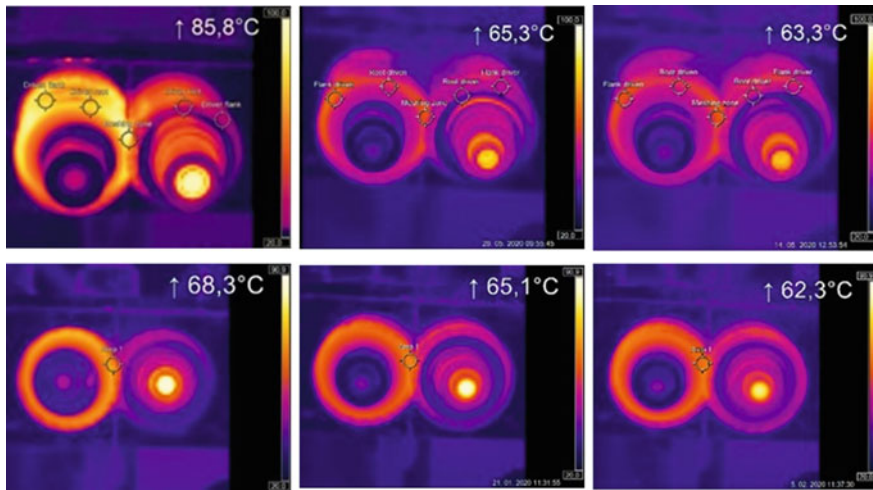


Fig. 7 Thermal camera snapshots for the meshing 42CrMo4/POM gear pairs in a stable region, $T = 1,5 \text{ Nm}$ (left); $T = 1,3 \text{ Nm}$ (centre); $T = 1,1 \text{ Nm}$ (right); E-gear (above), S-gear (below)

4.3 Optical Observation

The purpose of optical observations is to detect forms of gear failure in provided experiments. VDI 2736, Part 1 describes thermal overheating, root fracture, flank fracture, pitting, wear, and deformation as damage forms of plastic gears [17]. Worn gears exhibit at least some of the above-mentioned failure forms. And it is reasonable to expect to some extent different prevailing failure forms depending on load of gears with the same material combination.

The worn involute and S-gear after being loaded by 1.5 Nm until failure were examined optically to observe visible signs of damage. So, several photos were taken from the gear front, back, and face side. Some of the remaining teeth have rather long root and flank cracks, which are always near the pitch circle, which can be detected from the front side (seen by an observer when mounted on the testing rig). Some flank wear and flexural deformation appear as well. Tooth tips are also worn. And there are signs of thermal damage of flanks. From the back side, almost all teeth have rather long flank cracks, which initially proceed in the circumferential direction and then change the direction towards the opposite root. Some of root cracks spread over the entire face width. Figure 8 shows damage forms of the worn E-gear after its failure.

Damage forms of the S-gear run under the same conditions as E-gear pair are represented in Fig. 9. The front view shows regular, rather long cracks in the pitch circle zone or slightly below. Lower wear and flexural deformation, and some thermal damage are also present. Only several short root cracks can be observed from the rear side.

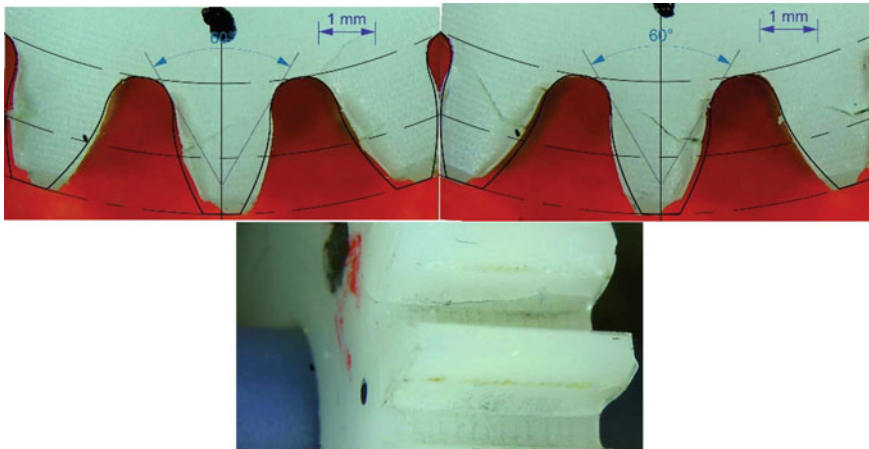


Fig. 8 Failure modes of the E-gear after experiment with load 1.5 Nm. (front—left, back—right, face side—below)

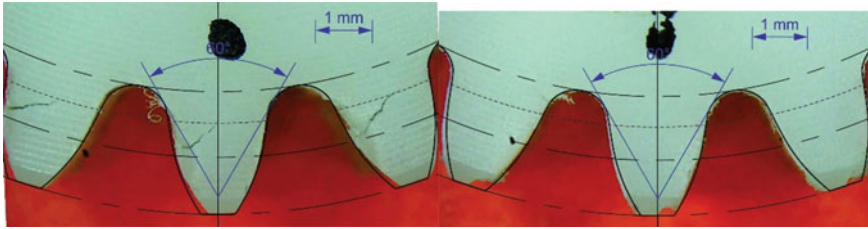


Fig. 9 Failure modes of the S-gear after experiment with load 1.5 Nm. (front—left, back—right)

4.4 Wear Measurement

It is necessary to access wear data quantitatively, and if possible, to access wear rate along the gear tooth flank. The basic idea is to detect a shape of a new plastic gear teeth shape and compare this reference shape to the worn gear teeth shapes. This can be done in successive manner as a process proceeds. Such an analysis is facilitated by an optical 3D measurement microscope, Alicona Infinite Focus SL. The Alicona 3D microscope is also used for precise measurements of cutting tools wear [18].

Some preliminary results for POM gears of both gear types are presented in Fig. 10 for the E-gear and in Fig. 11 for the S-gear. Two samples were scanned, both gears were loaded by torque of 1.1 Nm. The S-gear failed after 7.851×10^6 cycles and the E-gear after 7,780,156 cycles. Comparison of the new and the worn profile for both gear types shows severe wear. It appears as if fatigue is principal with higher loads and wear with lower loads.

So, wear development of the same gear pair during several stages from the new to the failed polymer gear is of interest. This can be processed for various loads from 1.5 down to 1.0 Nm or even lower. This is time consuming and a task to be accomplished later this year together with wear analysis according to VDI 2736. First results for the POM gears of both gear types loaded by 1.5 Nm, after 0.58×10^6 cycles are presented in Fig. 12. So, amount of wear for e.g., tip circle, pitch circle, active dedendum limit, etc. could be easily deducted. Some more wear is produced in E-gear pair in this case.

5 Conclusion

The presented chapter deals with testing and comparing E- and S-gears. S-gears are defined with a half parabolic function of the rack flank, which then defines a single path of contact which then defines external and internal gear geometry with any number of teeth. The height parameter a_p and the exponent n (form parameters) or the initial pressure angle α_w in C facilitate shaping of the gear, which was demonstrated in the chapter. Thermal properties of S-gears, i.e., their advantage over E-gears is in the fact that the former mesh with less sliding and more rolling, so S-gears reveal less frictional force and frictional losses or heat.

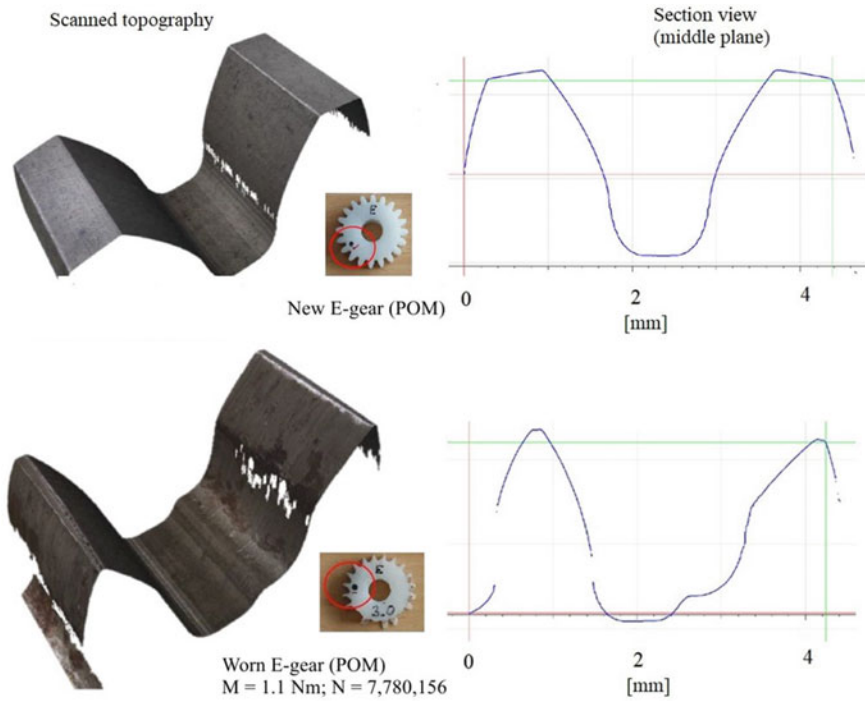


Fig. 10 E-gear teeth profile of the new (above) and worn gear (below)

The basic aim of durability tests, thermal and wear behaviour of gears made of various polymer materials and materials with fillers (fibres, stabilizers, lubricants, etc.) is to create a knowledge base which would facilitate proper material selection for demanding applications. As well it is necessary to improve knowledge on differences between E- and S-gear behaviour in applications.

The examined gear pairs were a combination of an alloy steel driving gear and a driven POM gear (POM contained some heat resistant additives). The tests with loads of 1.5, 1.3 and 1.1 Nm were repeated at least three times. They were conducted on small testbenches with thermal camera coverage and data logging. The testbench automatics registered failure time. There was a clear distinction between the S- and E-gears in favour of the former. Also, thermal characterization of S- and E-gears, based on continuous thermal records of the meshing, root, and flank areas of both gears, always shows lower temperatures of S-gears.

Regarding failure mechanisms, qualitative optical observations show fatigue cracks and fractures in root and flank area, flexural deformation, and wear. So, a tool for quantitative assessment was used, i.e., a precise 3D measurement microscope. 3D scanning is off-line, so the testing process is interrupted. First results are presented in the paper and show less wear of the S-gears, which could be attributed to lesser friction. The systematic research of wear started recently to improve the

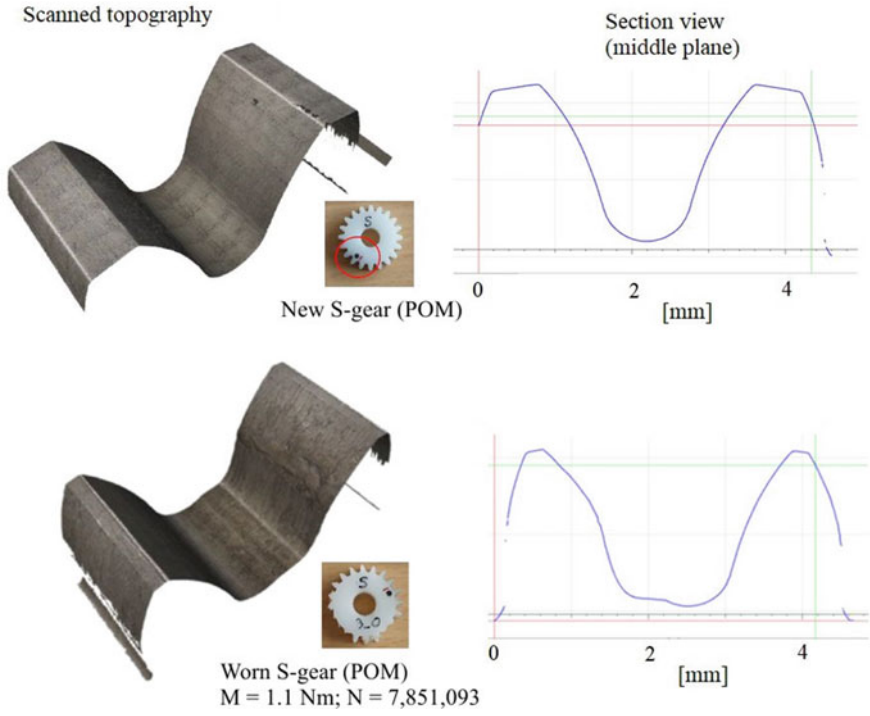


Fig. 11 S-gear teeth profile of the new (above) and worn gear (below)

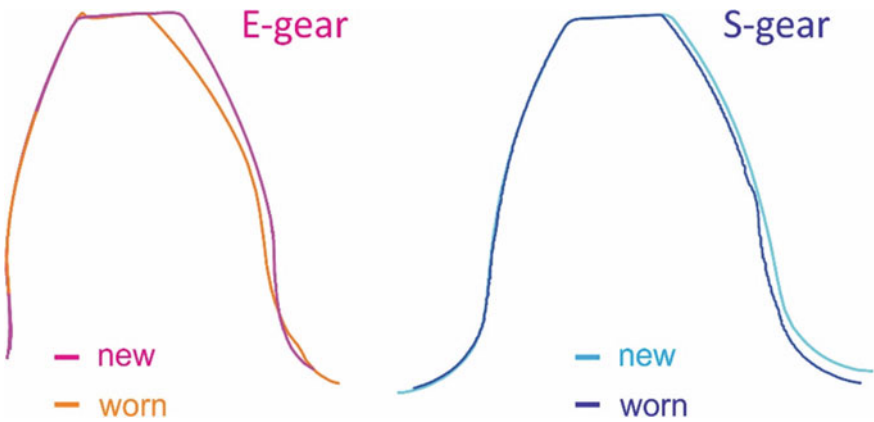


Fig. 12 S-gear teeth profile of the new (above) and worn gear (below)

understanding of the wear mechanisms and influences, e.g., gear geometry, load, number of cycles, etc.

The basic aim of durability tests, thermal and wear behaviour of gears made of various polymer materials and materials with fillers (fibres, stabilizers, lubricants, etc.) is to create a knowledge base which would facilitate proper material selection for demanding applications. As well it is necessary to improve knowledge on differences between E- and S-gear behaviour in applications.

Acknowledgements The investment is co-financed by the Republic of Slovenia and the European Union under the European Regional Development Fund, no. SME 2/17-3/2017 and C3330-18-952014.



EUROPEAN UNION
EUROPEAN REGIONAL
DEVELOPMENT FUND



REPUBLIC OF SLOVENIA
MINISTRY OF ECONOMIC DEVELOPMENT AND
TECHNOLOGY

References

1. Hlebanja, J., Hlebanja, G.: Spur gears with a curved path of contact for small gearing dimensions. In: International Conference on Gears, Garching near Munich, Germany, 4.-6.10.2010: Europe invites the world, (VDI-Berichte, ISSN 0083-5560, 2108). Düsseldorf: VDI-Verlag, pp. 1281–1294 (2010)
2. Hlebanja, J., Hlebanja, G.: Anwendbarkeit der S-Verzahnung im Getriebebau: Nichtevoventische Verzahnungen weiterentwickelt. Antriebstechnik, ISSN 0722-8546, 2005, 44(2), 34–38 (2010)
3. Hlebanja, G.: Specially shaped spur gears: a step towards use in miniature mechatronic applications. In: Miltenović, V. (ed.) Proceedings, The 7th International Scientific Conference Research and Development of Mechanical Elements and Systems—IRMES 2011, 27.-28.4.2011, Zlatibor, Mechanical Engineering Faculty, pp. 475–480 (2011)
4. Hlebanja, G., Hlebanja, J.: Recent development of non-involute cylindrical gears. In: Dobre, G., Vladu, M.R. (eds.) Power Transmissions: Proceedings of the 4th International Conference, Sinaia, Romania, June 20–23, 2012, (Mechanisms and machine science, ISSN 2211-0984, ISSN 2211-0992, vol. 13, pp. 83–98). Dordrecht [etc.]: Springer. cop. 2013 (2012)
5. Hlebanja, G., Hlebanja, J.: Influence of axis distance variation on rotation transmission in S-gears: example on heavy duty gears. In: International Conference on Gears, 7–9.10.2013, Garching (near Munich), pp. 669–679. Germany: Europe invites the world, (VDI-Berichte, ISSN 0083-5560, 2199). Düsseldorf: VDI-Verlag. cop. 2013 (2013)
6. Hlebanja, G., Kulovec, S., Zorko, D., Hlebanja, J., Duhovnik, J.: Influence of the tooth flank shape on thermal load of the gear. In: Europe invites the world, International Conference on Gears, International Conference on Gear Production, International Conference on High Performance Plastic Gears, Technische Universität München, Garching, Sept. 13–15, (VDI-Berichte, ISSN 0083-5560, 2294.2). Düsseldorf: VDI. 2017, pp. 1583–1592 (2017)
7. VDI 2736: Part 4. Thermoplastic gear Wheels: Determination of Strength Parameters on Gears. VDI-Richtlinien. Düsseldorf (2016)
8. Pogačnik, A.: Web demo 27.09.2018 – Plastic gear calculation. KissSoft (2018). https://old.kisssoft.ag/english/webdemos/downloads/plastic-gears/WebDemo_EN.pdf

9. VDI 2736: Part 2. Thermoplastic gear Wheels: Cylindrical gears Calculation of the load-carrying capacity. VDI-Richtlinien. Düsseldorf (2014)
10. Hlebanja, G., Kulovec, S., Hlebanja, J., Duhovnik, J.: On endurance of the S-shaped plastic gears. In: Simonovski, P., Rizov, T. (eds.) Proceedings: Balkan Association on Power Transmission Conference 2016: Faculty of Mechanical Engineering, Skopje, pp. 79–86 (2016)
11. Hlebanja, G., Hriberšek, M., Erjavec, M., Kulovec, S.: Durability investigation of plastic gears. In: Power transmissions 2019, 6th International BAPT Conference Power Transmissions 2019, Varna, Bulgaria, June 19–22, 2019, vol. 287, pp. 1–9 (MATEC web of conferences, ISSN 2261-236X). [Paris]: EDP Sciences (2019)
12. Hlebanja, G., Hriberšek, M., Erjavec, M., Kulovec, S.: Experimental determination of plastic gear durability. In: Marjanović Zulim, N. (ed.) IRMES 2019 Kragujevac, 5–7 September 2019, Kragujevac, (IOP Conference Series. Materials Science and Engineering (Online), ISSN 1757-899X, vol. 659, no. 1). [Kragujevac: Faculty of Engineering, 2019], vol. 659, no. 1, f. 1–11, <https://iopscience.iop.org/article/10.1088/1757-899X/659/1/012066> (2019). <https://doi.org/10.1088/1757-899X/659/1/012066>
13. Zorko, D., Kulovec, S., Tavčar, J., Duhovnik, J.: Different teeth profile shapes of polymer gears and comparison of their performance. *J. Adv. Mech. Design Syst. Manuf.* **11**(6), 1–10 (2017). <https://doi.org/10.1299/jamdsm.2017jamdsm0083>
14. Trobentar, B., Kulovec, S., Hlebanja, G., Glodež, S.: Experimental failure analysis of S-polymer gears. In: *Engineering Failure Analysis*, vol. 111 (104496), pp. 1–8. ISSN 1350-6307, April 2020. <https://doi.org/10.1016/j.engfailanal.2020.104496>
15. Hlebanja, G., et al.: Theory and Applications Based on S-gear Geometry, pp. xxx–xxx In: Radzevich, S.P., (ed.), *Recent Advances in Gearing: Scientific Theory and Applications*, 450 pages. Springer Nature, 2021. (in press, 2021)
16. Nieman, G., Winter, H.: *Maschinenelemente, Band II: Getriebe allgemein, Zahn-radgetriebe Grundlagen, Stirnrad Getriebe*. ISBN 3-540-11149-2. Springer Verlag, Berlin, Heidelberg, New York (1989)
17. VDI 2736: Part 1. Thermoplastic gear Wheels: materials, material selection, production methods, production tolerances, form design. VDI-Richtlinien. Düsseldorf (2016)
18. Grguraš, D., Kern, M., Pušavec, F.: Cutting performance of solid ceramic and carbide end milling tools in machining of nickel based alloy Inconel 718 and stainless steel 316L. In: *Advances in production engineering & management*, vol. 14, no. 1, pp. 27–38. ISSN 1854-6250, March 2019, http://apem-journal.org/Archives/2019/APEM14-1_027-038.pdf (2019). <https://doi.org/10.14743/apem2019.1.309>